Sixth International Symposium on Turbulence and Shear Flow Phenomena
Seoul, Korea, 22-24 June 2009

STUDY OF TURBULENT REACTING FLOW IN A JET ENGINE COMBUSTOR USING LARGE-EDDY SIMULATION

Donghyun You
Department of Mechanical Engineering,
Carnegie Mellon University
5000 Forbes Avenue, Pittsburgh, Pennsylvania 15213, USA
dhyou@cmu.edu

Frank Ham and Parviz Moin
Center for Turbulence Research,
Stanford University
488 Escondido Mall, Stanford, California 94305, USA
fham@stanford.edu, moin@stanford.edu

ABSTRACT

Large-eddy simulation (LES) is carried out to understand turbulent mixing, cooling, and combustion dynamics in a gas turbine engine combustor. An LES technique conserving discrete kinetic energy on arbitrary shaped unstructured grids is coupled with a Lagrangian particle tracking method for liquid fuel atomization and evaporation, and a presumed probability density function approach for turbulent combustion. A systematic analysis of the mean and turbulent flow fields elucidates dynamics of important flow structures and mechanisms for turbulent mixing and cooling. Predicted flow splits through the injector swirler and inner and outer dilution shrouds are in good agreement with experimental measurements. The mean temperature, temperature profile, and NO mole fraction at the exit of the combustor are also found to agree well with experimental data. The dilution jets produce significant magnitudes of the derivatives of the mean radial and circumferential velocity components, thereby dominating turbulent kinetic energy production. The present study suggests that combustor exit flow is highly unsteady and consists of small-scale velocity fluctuations and intermittent large-scale high temperature flow structures.

INTRODUCTION

The jet engine or gas-turbine engine combustors involve complex physical phenomena such as fuel spray break-up/evaporation/condensation, flow swirling, flow separation, turbulent mixing of main stream and dilution cooling air, and hot combustion products including pollutants. The mixing and cooling performance of a combustor dilution system can be implicated in thermal failure of the downstream turbine. Accurate observations and quantitative measurements of these processes in real industrial configurations are difficult and expensive. Better understanding of these flows for design modifications, improvements, and exploring fundamental physics demands high-fidelity numerical studies in real industrial configurations.

To date the engineering prediction of combustor flows in realistic configurations has relied on the Reynolds-averaged Navier-Stokes (RANS) equations (Malecki *et al.* 2001; Brankovic *et al.* 2001). In RANS, turbulence models for the Reynolds stress tensor provide time (or ensemble) averaged solution to the Navier-Stokes equations. Although computationally efficient, RANS-based approaches are in general not capable enough to predict unsteady large-scale turbulent fluid motions which dominate mixing, chemical reaction rate, and cooling. LES is considered attractive in predicting and understanding important flow features in combustors, since it resolves large-scale energetic turbulent motions which are mainly associated with the large-scale mixing and cooling. Kim & Syed (2004) and Mongia (2003) provide overviews on the importance and role of LES in designing advanced gas-turbine combustors.

The present paper focuses on understanding complex flow phenomena in a combustor realistic in terms of geometry and operation conditions. The accuracy and stability of numerical algorithms used for the present LES is achieved by conserving discrete kinetic energy as well as mass and momentum. Geometric complexity of practical combustors is overcome by the use of unstructured grids. Systematic validations of the present LES technique have been performed in the simulations of jets in cross flow, a model combustor with fuel spray, and flow through a rig-configuration of the Pratt & Whitney 6000 engine combustor. Some of these results have been reported in Moin & Apte (2007).

In the following sections, the computational methodology for simulating gas and liquid phase flows and results from LES of the Pratt & Whitney 6000 engine combustor are discussed in detail.

COMPUTATIONAL METHODOLOGY

Numerical Methods for Gas Phase

The numerical algorithm and solution methods are described in detail in Ham *et al.* (2006) and Moin & Apte (2007). The main features of the methodologies are summarized here. The spatially filtered governing equations for gas-phase are

$$(\overline{\rho}_g)_{,t} + (\overline{\rho}_g \widetilde{u}_j)_{,j} = \overline{\dot{S}}_m, \tag{1}$$

$$(\overline{\rho}_g \widetilde{u}_i)_{,t} + (\overline{\rho}_g \widetilde{u}_j \widetilde{u}_i)_{,j} = (2\overline{\mu}\widetilde{S}_{ij})_{,j} - (\tau_{ij})_{,j} - (\overline{p})_{,i} + \overline{\dot{S}}_i, \tag{2}$$

$$(\overline{\rho}_g \widetilde{Z})_{,t} + (\overline{\rho}_g \widetilde{u}_j \widetilde{Z})_{,j} = (\overline{\rho}_g \widetilde{\alpha}_Z (\widetilde{Z})_{,j})_{,j} - (q_{Z\,j})_{,j} + \overline{\dot{S}}_Z, \tag{3}$$

$$(\overline{\rho}_g \widetilde{C})_{,t} + (\overline{\rho}_g \widetilde{u}_j \widetilde{C})_{,j} = (\overline{\rho}_g \widetilde{\alpha}_C (\widetilde{C})_{,j})_{,j} - (q_{C\,j})_{,j} + \overline{\dot{\omega}}_C, \tag{4}$$

where the filtering operation is denoted by an overbar and Favre (density-weighted) filtering by a tilde. ρ_g, u_i, p, μ, and S_{ij} are the density, velocity, pressure, dynamic viscosity, and strain-rate tensor of gas-phase flow, respectively. Z and C are the mixture fraction and progress variable, respectively, while α_Z and α_C are molecular diffusivities of the corresponding scalars. $\dot{\omega}_C$ is the source term due to chemical reactions. The additional terms in the continuity, $\overline{\dot{S}}_m$, mixture fraction, $\overline{\dot{S}}_Z$, and momentum equations, $\overline{\dot{S}}_i$, are the interphase mass and momentum transport terms, which are obtained from the governing equations for spray droplet dynamics. The unclosed transport terms in the momentum and scalar equations are grouped into the residual stress τ_{ij} and residual scalar fluxes q_{Zj} and q_{Cj}. The choice of the progress variable C depends on the flow conditions and chemistry. Typically, the mass fraction of major product species is a good indicator of the forward progress of the reaction.

The Cartesian velocity components and pressure are stored at the nodes of the computational elements. A numerical method that emphasizes discrete energy conservation was developed for the above equations on unstructured grids with hybrid, arbitrary elements (Ham *et al.*, 2006). Controlling aliasing errors using kinetic energy conservation instead of employing numerical dissipation or filtering has been shown to provide good predictive capability for successful LES.

All terms in (1)-(4) are advanced using a second-order accurate fully-implicit method in time, and are discretized by the second-order central difference in space. A bi-conjugate gradient stabilized method (BCGSTAB) is used to solve the discretized momentum equations. The Poisson-type equation is solved by an algebraic multigrid method.

The combustion chemistry is incorporated in the form of a steady state one-dimensional flamelet model as in the flamelet/progresive-variable approach of Pierce & Moin (2004). The subgrid fluctuations in the mixture fraction, progress variable, and filtered combustion variables are obtained by integrating chemical state relationships over the joint probability density function (PDF) of Z and C. For example, the filtered chemical source term of the progress variable is given as

$$\overline{\dot{\omega}}_C = \int \dot{\omega}_C(Z,C)\widetilde{P}(Z,C)dZdC. \tag{5}$$

The joint subgrid PDF is modeled by writing $\widetilde{P}(Z,C) = \widetilde{P}(C|Z)\widetilde{P}(Z)$, where $\widetilde{P}(Z)$ is modeled by the presumed beta subgrid PDF and the conditional PDF $\widetilde{P}(C|Z)$ is modeled as a delta function. The governing equation for the mixture fraction in (3) consists of a source term due to the evaporation of liquid fuel spray. By assuming a beta PDF for $\widetilde{P}(Z)$, it is implicitly assumed that the timescale of evaporation is smaller than the timescale for the scalar mixing. From these assumptions, the flamelet library is computed and subgrid PDF integrals are evaluated to generate a lookup table which provides filtered variables as

$$\widetilde{f} = \widetilde{f}(\widetilde{Z}, \widetilde{Z''^2}, \widetilde{C}), \tag{6}$$

where $\widetilde{Z''^2}$ is the mixture fraction variance and $\widetilde{f}$ is a filtered variable such as the species mass fraction, temperature, dynamic viscosity, molecular diffusivities, and other properties required in the simulation. Nitric oxide (NO) formation is predicted by a model of Ihme & Pitsch (2007) that consists of the consideration of radiative heat losses and the additional solution of a transport equation for the NO mass fraction.

In (2)-(4), the eddy viscosity and eddy diffusivities are evaluated using the dynamic Smagorinsky model of Moin *et al.* (1991) while the subfilter variance of the mixture fraction is evaluated by the transported-filtered density function approach of Raman *et al.* (2005).

Numerical Methods for Liquid Phase

The liquid-phase fuel spray is simulated in a Lagrangian framework with an efficient particle tracking scheme on unstructured grids, which allows simulation of millions of independent droplet trajectories. The droplet motion is simulated using a version of the Basset-Boussinesq-Oseen equations:

$$\begin{aligned} \frac{d\mathbf{u_p}}{dt} &= D_{p_{drop}}(\mathbf{u_g} - \mathbf{u_p}) + \left(\mathbf{1} - \frac{\rho_\mathbf{g}}{\rho_\mathbf{p}}\right)\mathbf{g}, \\ \frac{d\mathbf{x_p}}{dt} &= \mathbf{u_p}, \end{aligned} \tag{7}$$

where

$$\begin{aligned} D_{p_{solid}} &= \frac{3}{4}C_d\frac{\rho_g}{\rho_p}\frac{|\mathbf{u_g} - \mathbf{u_p}|}{d_p}, \\ C_d &= \frac{24}{Re}(1 + 0.15Re_p^{0.687}), \end{aligned} \tag{8}$$

and the Basset force and added mass terms are neglected by the facts that the density ratio of the droplet to gas-phase fluid is about 10^3, droplet sizes are smaller than the turbulence integral length scale, and that the effect of shear on droplet motion is negligible. In (7) and (8), $\mathbf{x_p}$ is the position vector of the droplet centroid, $\mathbf{u_p}$ is the droplet velocity, $\mathbf{u_g}$ is the gas-phase velocity interpolated to the droplet location, ρ_p and ρ_g are the droplet and gas-phase densities, and $\mathbf{g}$ is the gravitational acceleration. The expression for solid-body drag in (8) is modified to account for droplet deformation and internal circulation (see Moin & Apte (2006) for more details).

The injected liquid jet/sheet is approximated by large drops with size equal to the initial annular film thickness. Then, a stochastic spray breakup model (Apte *et al.* 2003) generates a broad range of droplet sizes depending on Weber numbers. In this model, the characteristic radius of droplets is assumed to be a time-dependent stochastic variable with a given initial size distribution. The breakup of parent drops into secondary droplets is viewed as the temporal and spatial evolution of this distribution function around the parent-droplet size according to the Fokker-Planck (FP) differential equation (see Apte *et al.*, 2003). As new droplets are formed, parent droplets are destroyed and Lagrangian tracking in the physical space is continued until further breakup events.

Drop evaporation rates are estimated based on quasi-steady analysis of a single isolated drop in a quiescent environment. Multiplicative factors are then applied to consider the convective and internal circulation effects. The Lagrangian equations governing particle mass and heat transfer processes are

$$\begin{aligned} \frac{d}{dt}(m_p) &= -\dot{m}_p, \\ m_p C_{pl}\frac{d}{dt}(T_p) &= h_p\pi d_p^2(T_g - T_p) - \dot{m}_p\Delta h_v, \end{aligned} \tag{9}$$

where Δh_v is the latent heat of vaporization, m_p the mass of the droplet, T_p the temperature of the droplet, and C_{pl}

the specific heat of liquid. The diameter of the droplet is obtained from its mass, $d_p = (6m_p/\pi\rho_p)^{\frac{1}{3}}$. The effective heat transfer coefficient h_p is defined as $h_p = k_s(dT/dr)_{sg}/(T_g - T_s)$, where k_s is the effective conductivity of the surrounding gas at the droplet surface and the subscript s stands for the surface of the droplet.

Performing spray breakup computations using Lagrangian tracking of each individual droplet gives rise to a large number of droplets ($\approx 20 - 50$ million) in localized regions very close to the injector. In this study a novel hybrid particle-parcel scheme has been developed and is employed to reduce effectively the number of particles tracked and yet represent the overall spray evolution properly (see Moin & Apte, 2006 for details).

FLOW CONFIGURATION

The simulation is performed at cruise condition for a single injector shown in Fig. 1, which represents a 20° sector of the full combustor. The computational domain consists of pre-diffuser, fuel injector, swirler, and inner and outer dilution shrouds and holes. Liner cooling of the combustor chamber walls is modeled as transpiration boundary conditions. The Reynolds number based on inlet conditions and

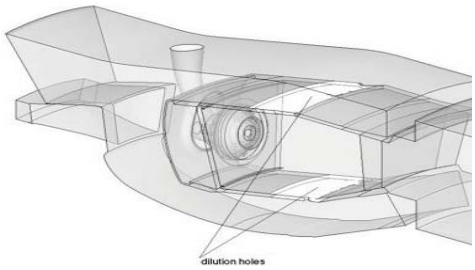

(a)

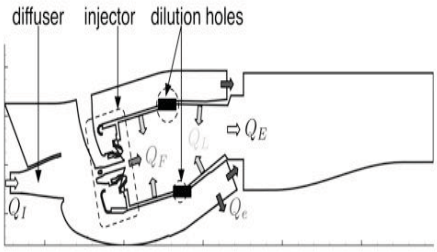

(b)

Figure 1: (a) Pratt & Whitney gas turbine engine combustor and (b) schematic diagram of flow configuration. The combustor geometry presented in this paper is scaled with arbitrary aspect ratios.

a reference length scale of 1 inch is around 500,000 and becomes 150,000 in the main (core) swirler channel.

Liquid fuel (Jet-A) is injected into the combustion chamber through an annular opening at the injector exit. These drops are convected by the surrounding hot air, then break and evaporate. The fuel vapor is mixed with the surrounding air producing non-premixed spray flames. The flow parameters for both gas- and liquid-phase flows are summarized in Table 1.

Two computational grids consisting of 3 million and 24 million hybrid elements are employed. The time step size is about $1 - 1.2$ micro-seconds for both mesh cases. In the 3 million mesh case, a combustor-flow-through time is about 14 hours on 80 CPUs of a 2.4GHz Intel XEON cluster, while, in the 24 million mesh case, it is about 19 hours on 512 CPUs of an 1.9 GHz IBM Power 5 at Lawrence Livermore National Laboratory. About 10 combustor-flow-through times are required to obtain first and second-order statistics.

Air flow	
Q_I	mass flow rate at the inlet of diffuser
Q_e	mass flow rate extracted through the casings $= 23.15\%Q_I$
Q_{IE}	mass flow rate inside combustor chamber $= Q_I - Q_e = 76.85\%Q_I$
Q_L	mass flow rate through the liner $= 24.3\%Q_{IE}$
Q_F	mass flow rate through the injector $= 8.67\%Q_{IE}$
Liquid fuel spray	
fuel-air-ratio	$=$ far $= 0.027$
stoichiometric coefficient	$=$ far$/0.068 = 0.395$
mass flow rate	$= 0.019$ kg/s
axial velocity of fuel injection	$= 3.56$ m/s
tangential velocity of fuel injection	$= 3.56$ m/s

Table 1. Boundary conditions for air flow and liquid fuel spray.

RESULTS AND DISCUSSION

Gross Features of Flow Field

Gross features of reacting flow in the combustor are illustrated in Fig. 2, which shows an instantaneous snapshot of iso-surfaces of temperature and fuel sprays swirling with a conical distribution. The reacting flow simulation

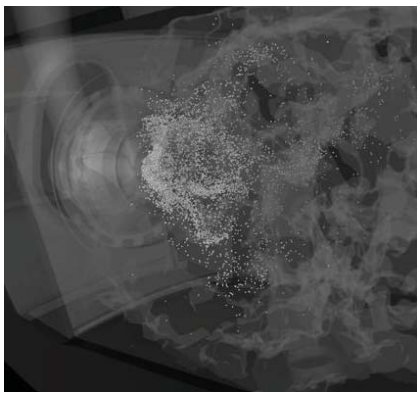

Figure 2: Snapshot of iso-surfaces of temperature and fuel sprays.

was started by first simulating non-reacting flow with spray undergoing breakup. Once spray particles are sufficiently injected into the chamber, the air-fuel mixture is ignited to start a reacting flow simulation. Then the total number of

spray particles becomes statistically steady by the balance between spray evaporation and injected fuel flow rate and breakup.

Contour plots of the mean velocity components obtained on 3 million and 24 million mesh elements in the symmetry $x-y$ plane are shown in Fig. 3. Compressed air enters the pre-diffuser of the combustor and is split to enter in part into the swirler and in part into the inner and outer dilution shrouds. The swirling flow near the injector generates helical motions of vortical structures and flow reversal in the core of the swirling flow. Multiple dilution jets are produced through the lower and upper dilution holes by the pressure difference between the dilution shrouds and combustor chamber. Flow swirling near the injector and dilution-jet mixing are found to be sensitive to mesh resolution. On a 24 million mesh, the size of flow recirculation near the injector is found to be larger than that in the 3 million mesh case.

Similarly, the instantaneous and mean temperature and the root-mean-squared temperature fluctuations are sensitive to mesh resolution in the swirl and mixing zones (Fig. 4). The mean temperature is found to be drastically reduced by the dilution jets while high temperature fluctuations are especially noticeable along the dilution jets and near the wall in the recirculation zone.

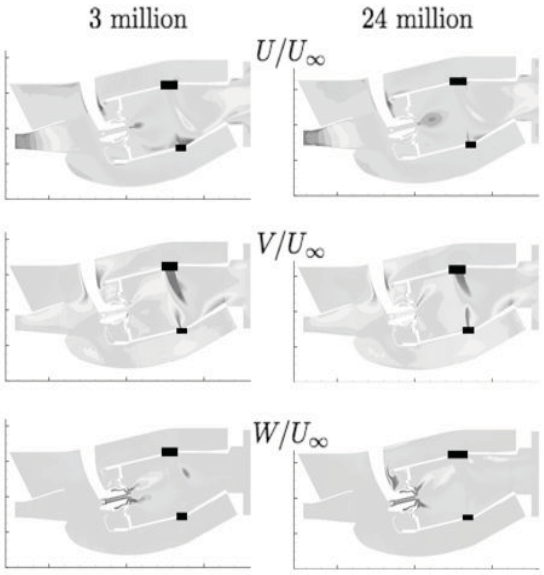

Figure 3: Contour plots of the mean velocity components in the symmetry $x-y$ plane. Red (blue) colored regions correspond to positive (negative) velocity. Figures are distorted.

Validation

The inflow entering the pre-diffuser is split through the front end swirler and outer dilution (OD) and inner dilution (ID) shrouds. The flow splits predicted by the present LES are found to be less sensitive to mesh resolution and are in excellent agreement with experimental data as shown in Fig. 5.

The normalized temperature profile averaged over the time and circumferential direction at the combustor exit plane is in close agreement with the experimental data as shown in Fig. 6. The LES simulations predict a rise in temperature near the outer casing of the combustor similar to

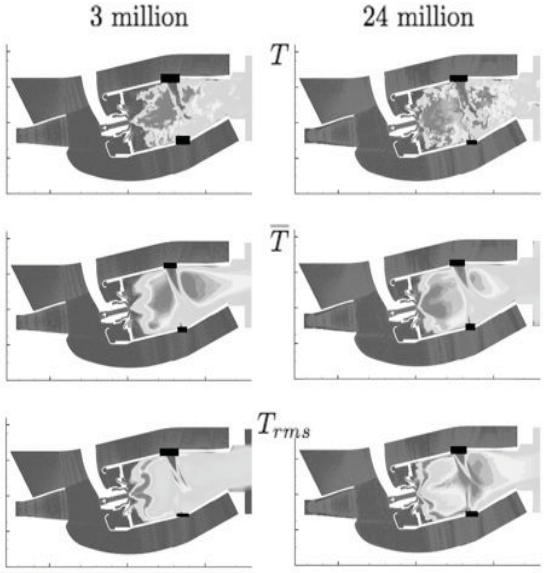

Figure 4: Contour plots of the instantaneous, mean, and rms temperature in the symmetry $x-y$ plane. Red (blue) colored regions correspond to high (low) magnitudes of temperature and rms temperature. Figures are distorted.

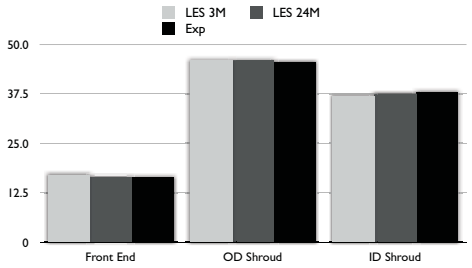

Figure 5: Flow splits in the combustor. Black: LES on 24 million mesh; brown: LES on 3 million mesh; grey: experiment.

the experimental data. It is found that the temperature profile predicted on a 24 million mesh is closer to the experimental data near the outer casing.

As summarized in Table 2, the time and plane averaged temperature at the exit plane is predicted to be 4% and 2% higher than the experimental value in the 3 million and 24

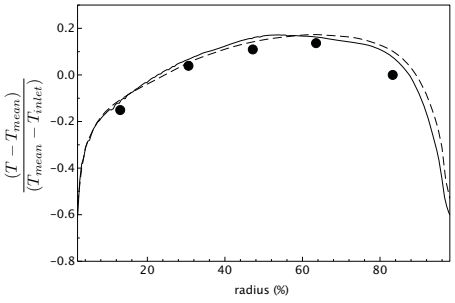

Figure 6: Mean temperature profile at the exit plane of the combustor. Solid line, LES on a 24 million mesh; dashed line, LES on a 3 million mesh; circle, experiment.

Case	3 million	24 million
T_{LES}/T_{EXP^*}	1.04	1.02
NO_{LES}/NO_{EXP^*}	1.24	1.10

Table 2: Averaged meant temperature and NO mole fraction at the combustor exit plane. *Experimental data by Pratt & Whitney.

million cases, respectively. The NO mole fraction predicted on a 3 million mesh is also in reasonable agreement with the experimental value, while the prediction on a 24 million mesh is in progress and will be presented at the conference.

Turbulent Mixing and Cooling

As shown in Fig. 7(a), near the injector, the flow field is dominated by swirling large-scale coherent vortical structures with high temperature. The large-scale swirling coherent vortical motions are destroyed once the swirling main stream encounters cross-stream dilution jets introduced from upper and lower dilutions holes (Fig. 7(b)). As shown in Fig. 8, the present LES indicates that derivatives of the mean radial and circumferential velocity components dominate turbulent kinetic energy production in the mixing zone of main stream and dilution jets. Influenced by the dilution-jet mixing, at the exit of the combustor as shown in Fig. 7(c), the velocity field is mainly characterized as small-scale less coherent flow motions, while the temperature field is dominated by intermittent large-scale high temperature flow structures.

Influence on Downstream Turbine

The large-scale high temperature flow structures have a direct influence on thermal safety of the downstream turbine. A thorough understanding of the mean and turbulent characteristics of the exit temperature is, therefore, essential in designing a highly efficient turbine cooling system. The present LES indicates that, in the the present combustor configuration, the downstream turbine blades should be prepared for the peak mean temperature around the mid-span region as shown in Fig. 9(a). At the same time, significant temperature fluctuations are observed near the casings of the combustor as shown in Fig. 9(b). These peak rms values at hub and tip gap may have implications on the thermal fatigue of turbine blades.

CONCLUSIONS

Large-eddy simulation of turbulent reacting flow in an aircraft jet engine combustor has been conducted to elucidate mechanisms of turbulent mixing and cooling and potential implications on thermal issues of the downstream turbine. Detailed chemical reactions, spray dynamics, and the interaction between gas- and liquid-phase flows have been predicted on a coupled Eulerian (for gas-phase flow) and Lagrangian (for liquid phase flow) framework equipped with a flamet/progress-variable approach for combustion. Mesh resolution effect on the LES solution has been examined by employing two different meshes consisting of 3 million and 24 million elements. Flow and temperature fields at the exit of combustor are reasonably well predicted even on a coarse mesh (3 million elements) while more detailed flow features such as swirl flow and dilution-jet mixing are better captured on a finer mesh (24 million elements). Flow splits through the combustor and the mean temperature, temperature profile, and NO mole fraction at the exit of the combustor are predicted to be in favorable agreement with experimental data. The present study suggests that turbulent kinetic energy production is dominated by strong derivatives of the mean radial and circumferential velocity components in the dilution-jet mixing zone and the combustor exit flow consists of fine-scale velocity fluctuations and intermittent large-scale high temperature flow structures. It is found that turbine blades may suffer from thermal fatigue due to highly fluctuating temperature, especially near the casing walls.

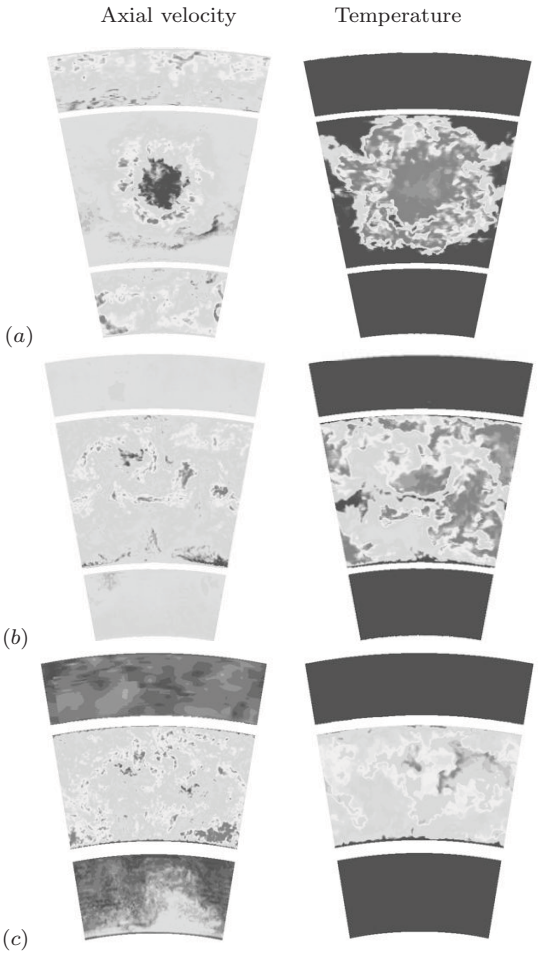

Figure 7: Contour plots of the instantaneous axial velocity and temperature in radial-circumferential planes at three axial locations. (a) $x/L_{ref} = 1$; (a) $x/L_{ref} = 4$; (c) $x/L_{ref} = 6$. See Fig. 1(b) for the axial locations. Figures are scaled with an arbitrary aspect ratio.

ACKNOWLEDGMENTS

The authors gratefully acknowledge the support from the U.S. Department of Energy Advanced Simulation and Computing program and provision of experimental data and jet-engine configuration from Pratt & Whitney. The authors are also grateful to Professors Iaccarino and Pitsch for their valuable contributions.

REFERENCES

Apte, S., Gorokhovski, M. and Moin, P., 2003, "LES of atomization spray with stochastic modeling of secondary breakup", *International Journal of Multiphase Flow*, Vol. 29 (9), pp. 1503-1522.

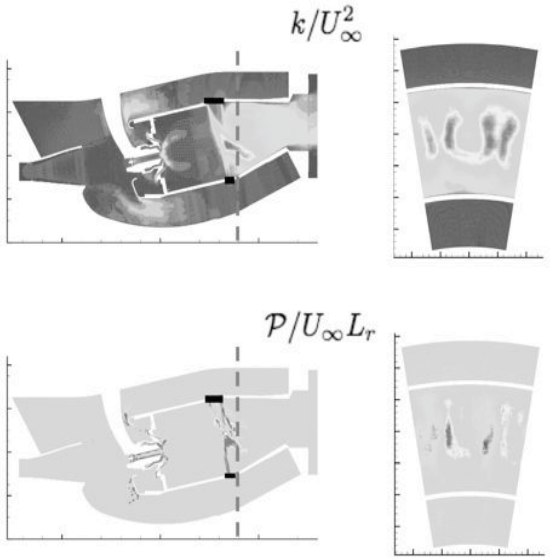

Figure 8: Contour plots of the turbulent kinetic energy and turbulent kinetic energy production in the symmetry $x-y$ plane and a circumferential $y-z$ plane at the location marked with a dashed line.

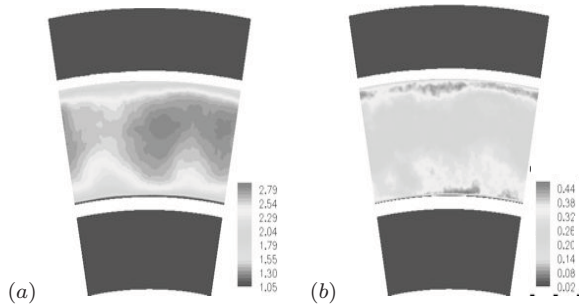

Figure 9: Contour plots of the (a) mean and (b) rms temperature in a radial-circumferential plane at $x/L_{ref} = 6$. Simulation on a 24 million mesh. Figures are scaled with an arbitrary aspect ratio.

Brankovic, A., McKinney, R. G., Ouyang, H., Porter, L., Kenndy, J., Madabhushi, R. and Colket, M., 2001, "Comparison of measurements and predictions of flow in a gas turbine engine fuel nozzle", *AIAA Paper 2001-0331*.

Ham, F., Mattsson, K. and Iaccarino, G., 2006, "Accurate and stable finite volume operators for unstructured flow solvers", *Annual Research Briefs*, Center for Turbulence Research, pp. 243-261.

Ihme, M. and Pitsch, H., 2007, "Pollutant formation and noise emission in turbulent non-premixed flames", *TF-Report 104*, Department of Mechanical Engineering, Stanford University.

Kim, W.-W. and Syed, S., 2004, "Large-eddy simulation needs for gas-turbine combustor design", *AIAA Paper 2004-0331*.

Malecki, R. E., Rhie, C. M., Colket, M. B., Madabhushi, R. K., McKinney, R. G., Ouyang, H., and Syed, S. A., 2001, "Application of an advanced CFD-based analysis system to the PW6000 combustor to optimize exit temperature distribution - Part I: Description and validation of the analysis tool", *ASME Paper 2001-GT-0062*.

Moin, P. and Apte, S.V., 2006, "Large-eddy simulation of realistic gas turbine combustors", *AIAA Journal*, Vol. 44 (4), pp. 698-708.

Moin, P., Squires, K., Cabot, W. and Lee, S., 1991, "A dynamic subgrid model for compressible turbulence and scalar transport", *Physics of Fluids A*, Vol. 3 (3), pp. 2746-1757.

Mongia, H., 2003, "Recent advances in the development of combustor design tools", *AIAA Paper 2003-4495*.

Pierce, C.D. and Moin, P., 1998, "A dynamic model for subgrid-scale variance and dissipation rate of a conserved scalar", *Physics of Fluids*, Vol. 10 (12), pp. 3041-3044.

Pierce, C.D. and Moin, P., 2004, "Progress-variable approach for large-eddy simulation of turbulent non-premixed combustion", *Journal of Fluid Mechanics*, Vol. 504, pp. 73-97.

Raman, V., Pitsch, H. and Fox, R.O., 2005, "Hybrid large-eddy simulation/Lagrangian filtered-density-fuction approach for simulating turbulent combustion", *Combustion and Flame*, Vol. 143, pp. 56-78.